

VAQF: Fully Automatic Software-hardware Co-design Framework for Low-bit Vision Transformer

Mengshu Sun¹ Haoyu Ma² Guoliang Kang³ Yifan Jiang³ Tianlong Chen³ Xiaolong Ma¹
Zhangyang Wang³ Yanzhi Wang¹

Abstract

The transformer architectures with attention mechanisms have obtained success in Nature Language Processing (NLP), and Vision Transformers (ViTs) have recently extended the application domains to various vision tasks. While achieving high performance, ViTs suffer from large model size and high computation complexity that hinders the deployment of them on edge devices. To achieve high throughput on hardware and preserve the model accuracy simultaneously, we propose VAQF, a framework that builds inference accelerators on FPGA platforms for quantized ViTs with binary weights and low-precision activations. Given the model structure and the desired frame rate, VAQF will automatically output the required quantization precision for activations as well as the optimized parameter settings of the accelerator that fulfill the hardware requirements. The implementations are developed with Vivado High-Level Synthesis (HLS) on the Xilinx ZCU102 FPGA board, and the evaluation results with the DeiT-base model indicate that a frame rate requirement of 24 frames per second (FPS) is satisfied with 8-bit activation quantization, and a target of 30 FPS is met with 6-bit activation quantization. To the best of our knowledge, this is the first time quantization has been incorporated into ViT acceleration on FPGAs with the help of a fully automatic framework to guide the quantization strategy on the software side and the accelerator implementations on the hardware side given the target frame rate. Very small compilation time cost is incurred compared with quantization training, and the generated accelerators show the capability of achieving real-time execution for state-of-the-art ViT models on FPGAs.

1. Introduction

The attention mechanisms, especially the transformer architectures (Vaswani et al., 2017), have achieved remarkable progress in Nature Language Processing (NLP) in the past few years (Radford et al.; Brown et al., 2020). Recently, the Vision Transformer (ViT) structure (Dosovitskiy et al., 2020) firstly introduces the transformers into the image classification task and suggests that a convolution-free architecture can achieve state-of-the-art performance. Later on, transformers have been widely used in several vision tasks performance, such as detection (Carion et al., 2020; Zhu et al., 2020), segmentation (Zheng et al., 2020; Wang et al., 2020), and pose estimation (Lin et al., 2020; Li et al., 2021). However, the excellent performance improvement requires increasing the model size and computation complexity, and it is difficult to deploy these huge models into real-world applications like augmented reality and autonomous driving.

To address this issue, many efforts have been devoted to compressing the cumbersome transformer architectures into a lightweight counterpart, including knowledge distillation (Jiao et al., 2019; Sanh et al., 2019; Sun et al., 2019; Touvron et al., 2021), pruning (Michel et al., 2019; Chen et al., 2020; 2021c), and quantization (Zafir et al., 2019; Bai et al., 2020; Shen et al., 2020). Among all these compression techniques, quantization is a popular solution as it still preserves the original network architecture. Concretely, quantization aims to replace the 32-bit parameter with a low-bitwidth representation. In NLP, the recent Binary-BERT (Bai et al., 2020) pushes BERT quantization to the limit by weight binarization, and introduces quantization on activations to bring additional energy savings. However, compared with the one-hot tokens in language, the input image patches in vision contain richer information, and it is unclear whether the binarization is still effective in ViTs.

In this paper, we firstly introduce the binarization into vision transformers. As fully binarization will lead to significant accuracy loss for ViTs, we adopt binary precision for weights and low precision for activations. Different from Binary-BERT, our method directly applies the methods in 1-bit convolutions (Rastegari et al., 2016; Liu et al., 2020) to achieve the binary weights. To support the inference of quan-

¹Northeastern University ²University of California, Irvine

³University of Texas at Austin. Correspondence to: Mengshu Sun <sun.meng@northeastern.edu>.

tized ViT models on FPGAs, we propose a ViT Automatic Quantization Framework, namely VAQF, to generate ViT accelerators according to the real-time frame rate requirement. A compilation step is conducted to automatically determine the quantization precision for activations on the software side and the accelerator parameter settings on the hardware side when the model weights are compressed into binary format. From a specific activation precision, a set of accelerator parameters can be inferred, and the overall resource utilization and inference performance can thus be estimated in advance. If the estimated frame rate meets the target, then the corresponding activation precision is decided to guide the quantization process, and the corresponding accelerator settings are adopted for hardware implementations. Depending on the specific model structure and target frame rate, this compilation step costs several minutes to several hours, which is less than one tenth of the training time for quantization. As for the ViT accelerator, a general compute engine is included to handle both fully-connected (FC) layers with one matrix multiplication and multi-head attention layers performing the matrix multiplication for multiple times. Because of the binary weights, the quantized computations can be replaced with additions and subtractions, and are thus implemented with lookup tables (LUTs) on FPGAs. The computations along the output channel, input channel, and head dimensions are totally or partially pipelined following the accelerator settings. Besides, the data packing technique is adopted to mitigate the memory burden and improve the overall computation throughput of the implementations.

Specifically, when binarizing the weights, our quantized ViT can achieve 79.5% on the ImageNet-1K validation set, which is just a 2.3% performance drop compared with the full-precision model (81.8%) but brings 32 \times reduction in model size. When further quantizing the activations to 8-bit and 6-bit, our method can still achieve accuracy of 77.6% and 76.5%, respectively, which outperforms previous state-of-the-art lightweight ViTs. The accelerator implementations are developed with Vivado High-Level Synthesis (HLS) and evaluated on the Xilinx ZCU102 FPGA board with the DeiT-base model. The experimental results indicate that 8-bit activation quantization is necessary for an inference frame rate of 24 frames per second (FPS), and 6-bit activation quantization is needed for 30 FPS.

Our main contributions are summarized as follows:

- We firstly build the quantized vision transformer with binary weights and low precision activations and achieve new state-of-the-art performance compared with other lightweight ViTs.
- We propose VAQF, a fully automatic framework that guides both quantization training and FPGA mapping. Given the target frame rate, VAQF generates the re-

quired quantization precision and accelerator description for direct software and hardware implementations.

- We design a layer-specific optimization scheme, and comprehensive FPGA optimization techniques are utilized to fully explore the data efficiency, execution parallelism, and resource utilization that maximize the performance and achieve real-time execution for quantized ViT models.

The rest of the paper is organized as follows. Section 2 discusses the related work in ViT compression and inference acceleration on hardware. Section 3 provides an overall flow of VAQF. The ViT quantization methods are presented in Section 4, and the implementation details of ViT acceleration with quantization on FPGAs are introduced in Section 5. The experimental results are reported in Section 6. Finally, Section 7 concludes the paper.

2. Related Work

2.1. Vision Transformers

The Vision Transformer (ViT) architecture is firstly proposed in (Dosovitskiy et al., 2020), which uses the attention mechanism (Vaswani et al., 2017) to solve various vision tasks. Compared to traditional CNN structures that operate on a fixed-sized window with restricted spatial interactions (Raghu et al., 2021), ViT allows all the positions in an image to interact through transformer blocks. Since then, many variants have been proposed (Graham et al., 2021; Liu et al., 2021c; Yuan et al., 2021a; Wang et al., 2021b; Han et al., 2021; Wu et al., 2021; Chen et al., 2021b; Steiner et al., 2021; El-Nouby et al., 2021; Liu et al., 2021a; Wang et al., 2021a; Bao et al., 2021). For example, DeiT (Touvron et al., 2021), T2T-ViT (Yuan et al., 2021b) and Mixer (Chen et al., 2021d) tackle the data-inefficiency problem and make ViT trainable only with ImageNet-1K (Deng et al., 2009). PiT (Heo et al., 2021) proposes a pooling-based Vision Transformer architecture with a desirable spacial dimension for better model capability and generalization performance. LV-ViT (Jiang et al., 2021) introduces a token labeling approach to improve training. PS-ViT (Yue et al., 2021) abandons the fixed length tokens with progressive sampled tokens.

2.2. Transformer Quantization

Since the BERT era (Vaswani et al., 2017), quantization has been extensively studied to reduce the memory and computation complexity of the transformer architectures (Prato et al., 2019; Zafir et al., 2019; Shen et al., 2020; Zhang et al., 2020; Bai et al., 2020). In detail, (Zafir et al., 2019) finetunes the BERT with 8-bit quantization-aware training, and successfully compresses BERT with minimal accuracy loss. To avoid severe accuracy drop, (Shen et al., 2020)

uses the mixed-precision quantization. The later Ternary-BERT (Zhang et al., 2020) proposes to use approximation based and loss-aware ternarization to ternarize the weights in the BERT, and use distillation to further reduce the accuracy drop caused by lower capacity. The BinaryBERT (Bai et al., 2020) suggests that it is difficult to train a binary BERT directly due to its complex loss landscape, and proposes ternary weight splitting strategy to make the binary BERT inherit the good performance of the ternary one. However, all of them are designed for NLP, not for the computer vision tasks. The most recent work (Liu et al., 2021d) evaluates the post-training quantization on ViT and achieves comparable performance with full-precision ViT. However, they just push the compression ratio to $4\times$ (*i.e.* 8-bit) and the method is not tailored for acceleration on hardware like FPGAs.

2.3. Lightweight ViTs

Unlike CNNs, the ViT (Dosovitskiy et al., 2020) is typically more cumbersome and computationally extensive. Therefore, recently, lots of studies try to make ViT lightweight and efficient. These works usually revise the architecture of ViT (Touvron et al., 2021) and introduce the image-specific inductive bias of CNNs back into ViT (Wang et al., 2021b; Yuan et al., 2021b; Chen et al., 2021a) to reduce the number of parameters and complexity. In detail, the DeiT (Touvron et al., 2021) introduces the distillation token and applies knowledge distillation to transfer knowledge from pre-trained networks to lightweight ViTs. The T2T (Yuan et al., 2021b) proposes progressive tokenization to model the local structure information. The Cross-ViT (Chen et al., 2021a) uses a dual-branch transformer to combine image patches of different sizes to produce stronger image features, and propose a cross attention module to reduce computation. The MobileViT (Mehta & Rastegari, 2021) combines the strengths of CNNs and ViTs by replacing local processing in convolutions with global processing using transformers. All of these methods heavily modify the architecture of the standard ViT, while our quantized ViT still maintains the origin network architectures.

2.4. Transformer Acceleration on FPGAs

Model compression techniques has been applied and adjusted for transformer acceleration on hardware. The approach in (Li et al., 2020) leveraged block-circulant structure for weight representation and converted the matrix-vector multiplications in FC layers to FFT/IFFT computations on FPGA. Block-based weight pruning was applied to transformers in (Qi et al., 2021) with block-balanced sparsity and in (Peng et al., 2021) with column balanced block-wise sparsity. The balance in these methods means that the number of sparse rows or columns in each weight block is the same, or the number of sparse blocks along each column is kept the

same. This facilitates full computation resource utilization and high throughput of hardware implementations.

While pruning needs balanced sparsity for high resource usage efficiency, quantization is naturally more friendly to FPGA implementations. The method in (Liu et al., 2021b) employed 8×4 -bit and 8×8 -bit quantization on different parts of BERT. VAQF differs from previous work in the following aspects: 1) The quantization process is guided by the compilation step that determines the required activation precision given the target frame rate; 2) The precision for activation quantization is chosen from a wider range to meet a specific real-time frame rate requirement.

3. VAQF Overview

Figure 1 illustrates VAQF that builds an FPGA-based ViT inference accelerator. The ViT structure and desired frame rate (target FPS) are provided as input information. A compilation step is conducted to decide the required precision for activations with the accelerator settings to satisfy the FPS target, when the weights are binary. Specifically for an activation precision, a set of accelerator parameters can be inferred, and the overall resource utilization and inference performance can thus be estimated in advance. If the estimated frame rate meets the target, then the corresponding activation precision and accelerator settings are simultaneously decided. On the software side, this activation precision guides the quantization with the PyTorch library, as explained in Section 4, and the quantized ViT parameters are sent to the FPGA platform for model inferences. On the hardware side, the parameter settings are adopted for the accelerator, as described in Section 5. This compilation step costs several minutes to several hours depending on factors such as the target frame rate, the number of model layers, and the layer dimensions. Compared with quantization that takes days for training, the compilation time is small.

The accelerator description in C++ format is then generated and synthesized with the Vivado HLS tool. The rules of setting the accelerator parameters include the initial settings to maximize the computation parallelism under the specific precision, and the adjustments of parameters if the Vivado implementation fails because of placement or routing issues. The parameters may be slightly adjusted once or twice, and a successful implementation generates a bitstream file to be deployed on FPGAs. The synthesis and implementation for the accelerator take hours, which is also small compared with quantization training.

The key of this flow is to determine the required activation precision. For a baseline accelerator, 16-bit fixed-point numbers are used to represent the 32-bit floating-point parameters and activations of unquantized models without introducing accuracy loss. The activation precision will therefore

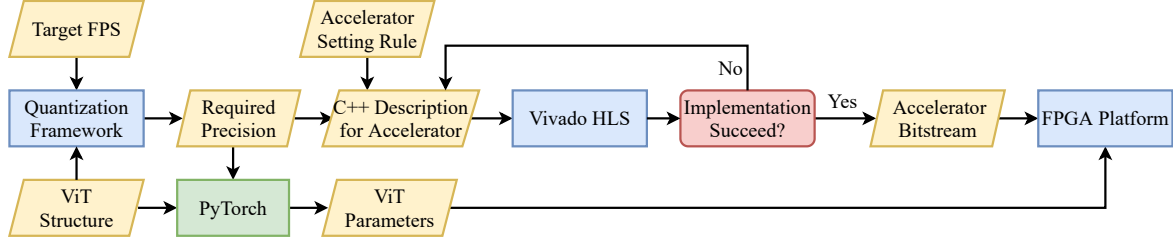


Figure 1. Overall Flow of VAQF.

be chosen from range 1 to 16 bits for higher throughput than the baseline design. As the frame rate has a reciprocal relationship with the total inference time of all the model layers, maximizing the frame rate is equivalent to minimizing the model inference time. The calculation of inference time will be elaborated in Section 5.3.3. The theoretical maximum frame rate for a ViT structure, denoted by FR_{max} , can be obtained supposing the activation precision is 1-bit, i.e., both weights and activations are binary. For a given target frame rate FR_{tgt} , the feasibility for accelerator implementation is first assessed by comparing FR_{tgt} with FR_{max} . $FR_{tgt} \leq FR_{max}$ means the accelerator supporting a frame rate no lower than FR_{tgt} can be implemented, and the appropriate precision is found through a binary search procedure. With a selection range of 1 to 16 bits, up to four rounds of search are conducted to find the required precision. In addition, if there exist multiple frame rate targets, all the possible precisions can be evaluated.

4. ViT Quantization Method

4.1. Preliminary: Vision Transformer

In this section, we revisit the architecture of the visual transformer (ViT). We give details about its each component.

Patch Embedding The ViT firstly processes a 2D image into a sequence of flattened 2D patches (Dosovitskiy et al., 2020) to adapt the 1D input sequence of the standard transformer. In detail, we denote the RGB image as $\mathbf{I} \in \mathbb{R}^{H \times W \times 3}$, where (H, W) is the resolution of the original image. \mathbf{I} is decomposed into $x_p \in \mathbb{R}^{N_p \times (3 \cdot P^2)}$, where P is the resolution of each patch, and $N_p = HW/P^2$ is the total number of patches. To fit the dimension of the hidden vector M , ViT applies a linear transformation $W \in \mathbb{R}^{(3 \cdot P^2) \times M}$ to project x_p into $\mathbf{X}_I \in \mathbb{R}^{N_p \times M}$. The ViT also appends the trainable [CLS] token $\mathbf{X}_{cls} \in \mathbb{R}^{1 \times M}$ to represent the global feature, and adds the learnable positional embeddings \mathbf{E}_{pos} to maintain positional information. Thus, the input to the transformer encoder can be represented as,

$$\mathbf{X}_0 = [\mathbf{X}_{cls}, \mathbf{X}_I] + \mathbf{E}_{pos} \in \mathbb{R}^{(N_p+1) \times M} \quad (1)$$

Where $[\dots]$ is the concatenation operation. For simplicity, we denote $F = N_p + 1$ as the total number of tokens.

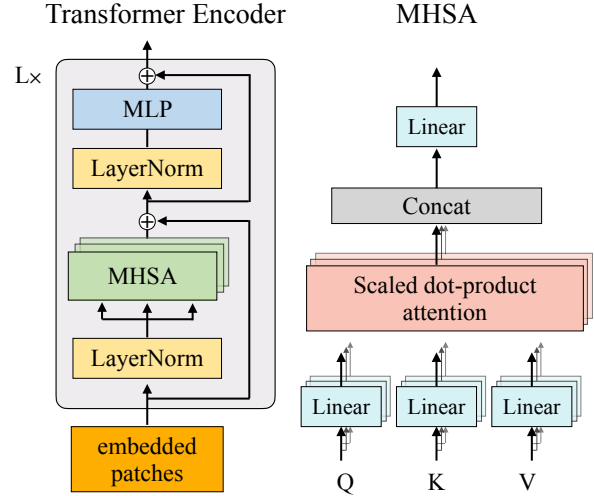


Figure 2. Illustration of transformer encoder.

Transformer Encoder Layers The transformer encoder includes several layers of multi-headed self-attention (MHSA) and multi-layer perceptron (MLP) blocks. The LayerNorm (LN) is applied prior to each block. Figure 2 shows the architecture of the transformer encoder layer, and operations in one encoder layer is summarized as:

$$\begin{aligned} \mathbf{X}'_l &= \text{MHSA}(\text{LN}(\mathbf{X}_{l-1})) + \mathbf{X}_{l-1}, \quad l = 1 \dots L \\ \mathbf{X}_l &= \text{MLP}(\text{LN}(\mathbf{X}'_l)) + \mathbf{X}'_l, \quad l = 1 \dots L \end{aligned} \quad (2)$$

In detail, the self-attention function aims to match a query and a set of key-value pairs to an output (Vaswani et al., 2017). Given input sequence \mathbf{X}_l , three linear projections $W_l^q, W_l^k, W_l^v \in \mathbb{R}^{M \times M_h}$ are firstly applied to transfer \mathbf{X}_l into the query $\mathbf{Q}_l \in \mathbb{R}^{F \times M_h}$, the key $\mathbf{K}_l \in \mathbb{R}^{F \times M_h}$, and the value $\mathbf{V}_l \in \mathbb{R}^{F \times M_h}$. The attention function is calculated by

$$\text{Softmax}(\mathbf{Q}_l \mathbf{K}_l^T / \sqrt{D}) \mathbf{V}_l \in \mathbb{R}^{F \times M_h} \quad (3)$$

Furthermore, for multi-head self-attention, N_h self-attention functions are applied to the input \mathbf{X} , and each of them produces an output sequence. The final output is the projection of the concatenated sequences. Typically, M_h is set

to M/N_h to maintain the consistency between the size of inputs and outputs.

The MLP block consists of two linear layers followed by a GELU activation. The first linear layer (with weights $W_l^{m1} \in \mathbb{R}^{M \times 4M}$) expands the dimension from M to $4M$, and the second layer (with weights $W_l^{m2} \in \mathbb{R}^{4M \times M}$) reduces it back to M .

Output Head Different from the pooling layers used in computer vision, ViT directly adds the output head upon \mathbf{X}_L^0 , which is the representation of the CLS token and serves as the embedding of the entire image. The output head is defined as:

$$y = \text{LN}(\mathbf{X}_L^0)W_{\text{out}}, \quad (4)$$

where $W_{\text{out}} \in \mathbb{R}^{M \times C}$, and C is the total number of classes.

4.2. ViT Quantization

Similar to (Liu et al., 2020; Bai et al., 2020), we binarize the weights in ViT, and reduce the activations into low-precision, to achieve the trade-off between efficiency and accuracy.

Binary Weights Following the definition in (Rastegari et al., 2016; Liu et al., 2020), given the matrices of real number weights \mathcal{W}_r , the matrices of binary weights \mathcal{W}_b are obtained by

$$w_b = \frac{\|\mathcal{W}_r\|_{l1}}{n} \text{Sign}(w_r) = \begin{cases} +\frac{\|\mathcal{W}_r\|_{l1}}{n}, & \text{if } w_r > 0 \\ -\frac{\|\mathcal{W}_r\|_{l1}}{n}, & \text{if } w_r \leq 0 \end{cases} \quad (5)$$

where w_r and w_b denote one specific element in the matrix \mathcal{W}_r and \mathcal{W}_b , respectively. $\frac{\|\mathcal{W}_r\|_{l1}}{n}$ is the scaling factor to minimize the difference between binary and real-valued weights. For ViT, all trainable weights in the transformer encoder layers belong to the linear transformation. Thus, we simply replace the weights from \mathcal{W}_r to \mathcal{W}_b in that linear layer to obtain the activations.

Progressive Binary Training As suggested by (Bai et al., 2020), training a binary BERT from scratch is challenging, as the loss landscape is steep. To alleviate this issue, we propose the progressive binary training strategy. Specifically, during the training process, we randomly select $p\%$ elements in \mathcal{W}_r , and only binarize these selected elements while keep other elements full-precision. $p\%$ is set to 0% at the beginning of the training, then it grows linearly with the increase of training epoch, and achieves 100% when the training process is completed. Therefore, \mathcal{W}_p consists of both binary weights and real-value weights during the training process. Specifically,

$$\mathcal{W}_p = M_p \cdot \mathcal{W}_b + (1 - M_p) \cdot \mathcal{W}_r, \quad (6)$$

where M_p is a mask with the same size as \mathcal{W}_r . During training, $p\%$ elements of the mask are set to 1, while the rest are 0.

Implementation Details Typically, both the first layer and the output head are not quantized in previous binary networks (Liu et al., 2020), as they are associated with the inputs and outputs. Similarly, we only consider quantizing the weights and activations within each transformer encoder, and for the patch embedding and the output head, full-precision weights and activations are utilized. Specifically, we binarize the weights in all attention layers (W_l^q , W_l^k , and W_l^v) and the weights in MLP layers (W_l^{m1} and W_l^{m2}) with Eq. (5). We consider a three-step training process: 1) Train a full-precision ViT from scratch and achieve the real-valued parameters; 2) Finetune the full-precision ViT with progressive binary training to obtain ViT with binary weights and full-precision activations; 3) Finetune the binary-weight model to quantize activations with desired precision.

5. Vision Transformer Acceleration on Hardware

In this section, we first discuss the optimization techniques for different types of computations in ViT layers (Sections 5.1 and 5.2), and then provide a detailed flow of optimizing the accelerator parameters given the model structure and desired frame rate (Section 5.3).

5.1. Compute Engine for Fully-Connected and Attention Layers

The implementation details of ViT acceleration on FPGA are displayed in Figure 3, and the notations of variables and parameters are listed in Table 1. As the storage and computation resources are limited on FPGA devices, the loop tiling technique is adopted to split the input, weight, and output data for each ViT layer into tiles, and tiling for an unquantized layer is shown as an example in Figure 3(a).

The most computation-intensive layers in ViTs include FC layers that exist in both multi-layer perceptron (MLP) modules and multi-head attention modules, and scaled dot-product attention layers that appear in multi-head attention modules. The primary computations of these two types of layers are both matrix multiplications. While an FC layer performs only one matrix multiplication, multi-head attention repeats the computations multiple times in parallel, so the accelerator is designed such that the computations can be executed in parallel across P_h attention heads. To make the design also compatible for FC computations, the N input channels in an FC layer are split into N_h groups, P_h of which are processed by the compute engine simultaneously at a time. A control signal is added to indicate whether the current layer is multi-head attention. For multi-head attention, the N_h heads of results are kept as they are, while for an FC layer, these results from N_h input channel groups are added together, making the final result for each output

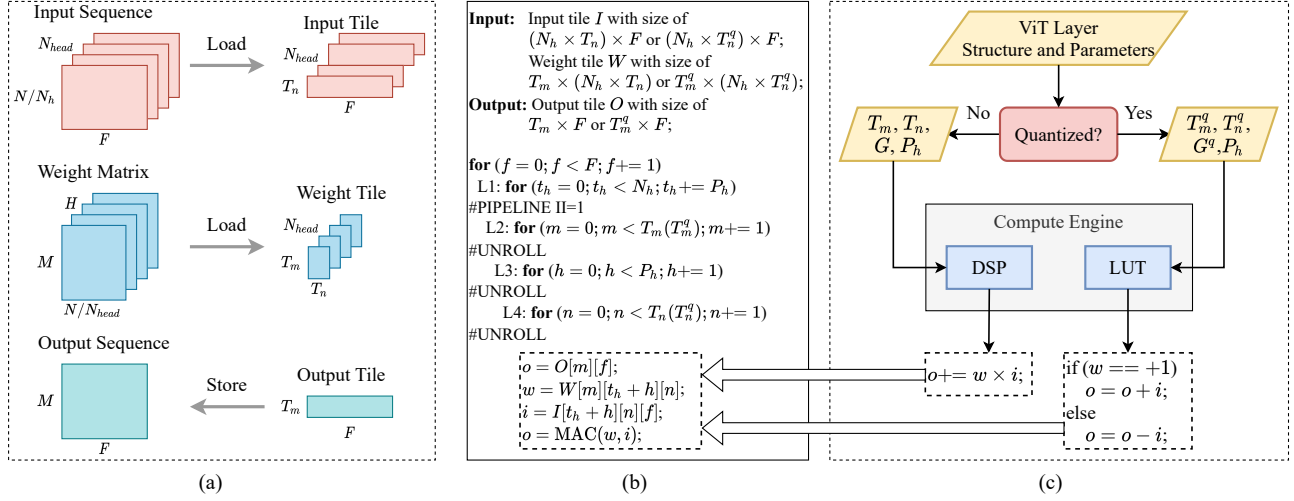


Figure 3. Detailed implementation of ViT accelerator. (a) Loop tiling of input, weight, and output for one model layer; (b) Computation flow in compute engine with loop tiling, pipelining and unrolling; (c) Processing flow of one model layer based on whether it is quantized or not.

Table 1. Notations for the ViT accelerator.

Notation	Description
M (N)	Number of output (input) channels
F	Number of token sequences
T_m (T_m^q)	Tiling size for unquantized (quantized) data in output channel dimension
T_n (T_n^q)	Tiling size for unquantized (quantized) data in input channel dimension
N_h	Total number of heads
P_h	Number of heads for computation in parallel
G (G^q)	Number of unquantized (quantized) data packed as one
S_{port}	Size of each AXI port on FPGA
p_{in} (p_{out}, p_{wgt})	Number of AXI ports used for data transfer of input (output, weight) tile
J_{in} ($J_{wgt}, J_{out}, J_{cmpt}$)	Number of clock cycles for input transfer (weight transfer, output transfer, computation) for a group of tiles
B_{in} (B_{out}, B_{wgt})	Number of BRAMs used by input (output, weight) tile
S_{bram} (S_{dsp}, S_{lut})	Available number of BRAMs (DSPs, LUTs) on FPGA

channel accumulated from all the input channels.

The main computation flow general for these two types of layers is displayed in Figure 3(b). The loops L2, L3, L4 under L1 are unrolled and pipelined so that the compute engine can manage $T_m \cdot P_h \cdot T_n$ multiply-accumulate (MAC) operations in parallel. For illustration simplicity of the MAC operation with the input and weight, the head and the input channel dimensions are shown separately. Figure 3(c) provides the processing flow of one ViT layer with or without quantization. The accelerator parameters needed for the compute engine include T_m (T_m^q), T_n (T_n^q), G (G^q), and

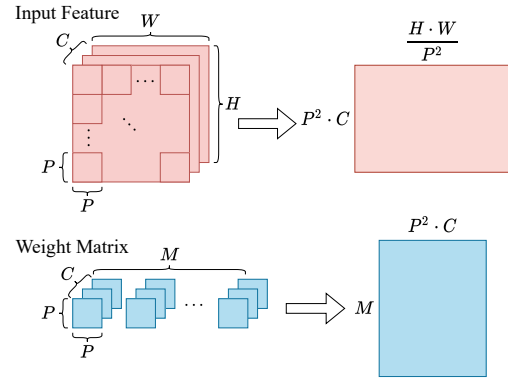


Figure 4. Conversion of input and weight tensors for the first convolutional layer.

P_h , the settings and adjustments of which are elaborated in Section 5.3. Unquantized computations with high precision are managed by the DSP resources on FPGA, whereas quantized computations can be replaced with additions or subtractions that would be managed by LUTs, since the weight value is binarized as either +1 or -1.

5.2. Processing of Other Layers in Vision Transformer

In addition to matrix multiplications in MLP and multi-head attention modules, ViTs contain convolution, scaling, softmax, activation, normalization, and skip-connection addition operations. The first layer of a ViT is a convolutional layer that can be converted to an FC layer, because its kernel size and stride is the same as the patch size P , meaning that the input data are used only once when a weight kernel slides across the input feature map, as shown in Figure 4,

where C , H and W denote the number of input channels, the height and width for the original input feature. The scaling, softmax, and GELU activation operations are performed on the host CPU of the FPGA, which introduces very small latency overhead for embedded FPGAs compared with matrix multiplications.

5.2.1. PROCESSING OF NORMALIZATION LAYERS AND SKIP-CONNECTIONS

In ViTs, layer normalization is applied at the beginning of each multi-head attention and each MLP module, and there is an identity skip-connection linking the input activations of each normalization layer and the output activations of the subsequent module, which can be seen from Figure 2. In the sequential processing of the layers, the inputs of the normalization layer require to be stored for later additions with the outputs of the following multi-head attention or MLP module. Since normalization layers are not so compute-intensive as FC ones, their parameters and inputs are not quantized but rather kept with higher precision, namely 16-bit on hardware to preserve the model accuracy. As a result, two data transfer ports are needed, one for the inputs of normalization that are stored as unquantized data, and the other for the outputs of normalization, also the inputs for the subsequent FC layer, which are stored as quantized data. It needs to be emphasized that the data transfer port for quantized FC inputs is necessary to minimize the input loading time for the FC layer as the input tiles would be loaded multiple times in the matrix multiplication with loop tiling.

5.3. Design of FPGA-Based Vision Transformer Accelerator

Before building the ViT accelerator supporting a specific frame rate, a baseline accelerator is realized for unquantized models, whose 32-bit floating-point parameters and activations are represented with 16-bit fixed-point numbers to reduce the computation and storage resource utilization without accuracy loss on hardware. Let us denote the optimized parameters for the baseline design as T_m^{base} , T_n^{base} and G^{base} . These parameters are treated as the starting point to find the required activation precision and optimize the ViT accelerator parameters.

Provided the target frame rate, VAQF will determine the proper activation precision, which is an inverse procedure, as the activation precision directly affects the accelerator settings and hence the actual frame rate. The following discussion of hardware implementation details is on the basis of a specific activation precision, but it does not mean the proper precision has been decided in the first step. Instead, it is found among several possible precisions after the analysis in terms of resource utilization and inference performance.

5.3.1. DATA PACKING

The data packing technique is employed to reduce the block RAM (BRAM) usage and the latency of data transfer between off-chip memory (DDR) and on-chip memory (BRAM). Although each BRAM on Xilinx FPGAs can accommodate 18k-bit data, the space of the whole BRAM might not be fully utilized, leading to high BRAM usage in the ViT acceleration implementation. This mainly results from loop pipelining and unrolling that requires each related data array to be partitioned into multiple smaller arrays. Data packing can mitigate this issue through concatenating multiple low-precision numbers as one number. With a data packing factor of G , the overall BRAM usage can be reduced by up to G times, and the number of clock cycles for input loading and output storage can be reduced by G times as well.

Each AXI port on FPGA with size S_{port} can accommodate G unquantized data or G^q quantized data. If $S_{port} = 64$, then $G = 4$ for 16-bit data used in our baseline design, and $G^q = 8$ if the quantization precision is 8-bit. A special case is when S_{port} cannot be divided exactly by the bit-length of quantized values. Take 6-bit quantization precision as an instance, $G^q = \lceil \frac{64}{6} \rceil = 10$, and only 60 of the 64 bits are exploited. Data packing is performed in the input channel dimension of the weights and input activations, and in the output channel dimension of the output activations. It is not displayed in Section 3(b) for illustration simplicity of MAC operation.

5.3.2. DETERMINING PARAMETERS FOR BEST COMPUTATION PARALLELISM

Although most layers of the ViT model are quantized, the first and last layers are not quantized to better maintain the model accuracy, and the accelerator compute engine still needs to handle unquantized data. As a result, we have two groups of accelerator parameters to be determined, i.e., T_m , T_n and G for unquantized layers, and T_m^q , T_n^q and G^q for quantized ones, while the parameter P_h remains the same in both situations. The ViT layers are handled one by one, so the accelerator will not perform unquantized computations and quantized ones simultaneously. Nonetheless, the same BRAMs for input, weight and output data can be utilized whether the layer is quantized or not. The related accelerator parameters are therefore decided to make the best effort to utilize the BRAMs.

When creating the ViT accelerator with support of quantization, the accelerator parameters for unquantized layers are first set as $T_n = T_n^{base}$ and $G = G^{base}$, and T_m is initially set to a value that is near to T_m^{base} and can be divided exactly by G and G^q . As mentioned in Section 5.3.1, G^q is directly calculated according to S_{port} and the required quantization

precision. T_n^q is then calculated by $T_n^q = \left\lceil T_n \cdot \frac{G^q}{G} \right\rceil$ for maximum utilization ratio of BRAMs for quantized data. P_h is usually a value that can divide N_h exactly. For instance, if $N_h = 6$, P_h is set to 3; if $N_h = 8$ or $N_h = 12$, then P_h is 4. In the next step, T_m^q is set as equal to T_m , and a hardware design with all these parameters is synthesized and implemented with Vivado HLS as an initial try. If the FPGA board cannot accommodate this design due to placement or routing issues (usually resulting from overutilization of LUTs), then T_m and T_m^q are adjusted for the implementation to fit into the board and minimize the overall inference latency as well. For low activation precision, T_m is reduced and T_m^q is increased until the FPGA resources are fully exploited. In this procedure, both T_m and T_m^q are kept as values that can be divided exactly by G and G^q for convenience of output storage.

5.3.3. PERFORMANCE ANALYSIS AND OBJECTIVE FUNCTION

The main variables in the equations in this section are explained in Table 1. For one layer i in ViT, the numbers of clock cycles needed for input tile loading, weight tile loading, and output tile storage are calculated as

$$\begin{aligned} J_{in} &= N_h \cdot \left((1 - \alpha) \cdot \left\lceil \frac{T_n}{G} \right\rceil + \alpha \cdot \left\lceil \frac{T_n^q}{G^q} \right\rceil \right) \cdot \left\lceil \frac{F}{p_{in}} \right\rceil, \\ J_{wgt} &= N_h \cdot \left((1 - \alpha) \cdot \left\lceil \frac{T_n}{G} \right\rceil + \alpha \cdot \left\lceil \frac{T_n^q}{G^q} \right\rceil \right) \cdot \left\lceil \frac{T_m}{p_{wgt}} \right\rceil, \\ J_{out} &= (1 + \gamma) \cdot \left((1 - \beta) \cdot \left\lceil \frac{T_m}{G} \right\rceil + \beta \cdot \left\lceil \frac{T_m^q}{G^q} \right\rceil \right) \cdot \left\lceil \frac{F}{p_{out}} \right\rceil, \end{aligned} \quad (7)$$

where α is 1 if the inputs and weights are quantized else 0, β is 1 if the outputs are quantized else 0, and γ is $N_h - 1$ if the current layer is a multi-head attention layer else 0. Additionally, the clock cycle number of computations for one group of tiles is

$$J_{cmpt} = F \cdot \left\lceil \frac{N_h}{P_h} \right\rceil. \quad (8)$$

The data loading and computation for the tiles are conducted simultaneously with the double buffering technique to overlap the data transfer with computations. The clock cycle number of this process is

$$J_{lc} = \max\{J_{in}, J_{wgt}, J_{cmpt}\}. \quad (9)$$

And to obtain the accumulation of output results, this process is performed multiple times. The clock cycle number for calculating the whole output tile is

$$\begin{aligned} J_s &= \max \left\{ J_{lc} \cdot \left((1 - \alpha) \cdot \left\lceil \frac{N}{N_h \cdot T_n} \right\rceil \right. \right. \\ &\quad \left. \left. + \alpha \cdot \left\lceil \frac{N}{N_h \cdot T_n^q} \right\rceil \right) + J_{cmpt}, J_{out} \right\}. \end{aligned} \quad (10)$$

The overall clock cycle number for a ViT layer i is therefore described by

$$J_i = \left((1 - \beta) \cdot \left\lceil \frac{M}{T_m} \right\rceil + \beta \cdot \left\lceil \frac{M}{T_m^q} \right\rceil \right) \cdot J_s + J_{out}. \quad (11)$$

With double buffering, the 18k-bit BRAM usage of the input, weight, and output tiles are given by

$$\begin{aligned} B_{in} &= 2 \cdot N_h \cdot \max \left\{ \left\lceil \frac{T_n}{G} \right\rceil \cdot \left\lceil \frac{F \cdot G \cdot 16}{18k} \right\rceil, \left\lceil \frac{T_n^q}{G^q} \right\rceil \cdot \left\lceil \frac{F \cdot G^q \cdot b^q}{18k} \right\rceil \right\}, \\ B_{wgt} &= 2 \cdot N_h \cdot \max \left\{ \left\lceil \frac{T_n}{G} \right\rceil \cdot \left\lceil \frac{T_m \cdot G \cdot 16}{18k} \right\rceil, \left\lceil \frac{T_n^q}{G^q} \right\rceil \cdot \left\lceil \frac{T_m \cdot G^q}{18k} \right\rceil \right\}, \\ B_{out} &= 2 \cdot N_h \cdot \max \left\{ \left\lceil \frac{T_m}{G} \right\rceil \cdot \left\lceil \frac{F \cdot G \cdot 16}{18k} \right\rceil, \left\lceil \frac{T_m^q}{G^q} \right\rceil \cdot \left\lceil \frac{F \cdot G^q \cdot b^q}{18k} \right\rceil \right\}, \end{aligned} \quad (12)$$

where b^q is the activation bit-width in quantization. As for the DSP utilization, since each DSP can manage one unquantized MAC operation with a 16-bit input and a 16-bit weight, the number of used DSPs is calculated by $T_m \cdot P_h \cdot T_n$ to perform $T_m \cdot P_h \cdot T_n$ MAC operations in parallel.

Finally, our objective function can be written as

$$\text{minimize} \quad \sum_i J_i \quad (13)$$

subject to

$$\begin{aligned} B_{in} + B_{wgt} + B_{out} &\leq S_{bram}, \\ T_m \cdot P_h \cdot T_n &\leq S_{dsp} \cdot r_{dsp}, \\ C_{lut} \cdot T_m^q \cdot P_h \cdot T_n^q &\leq S_{lut} \cdot r_{lut}, \end{aligned} \quad (14)$$

where r_{dsp} and r_{lut} are respectively the maximum ratio of DSPs and LUTs to be utilized for MAC operations, and C_{lut} is the LUT cost for one MAC with quantized operands. As mentioned in Section 3, minimizing the overall model latency is equivalent to maximizing the frame rate. If the maximum frame rate is no lower than the target frame rate, then the accelerator with the corresponding activation precision and parameter settings is feasible.

6. Evaluation

6.1. Experimental Setup

Datasets & Architectures We conduct all experiments on ImageNet-1K (Deng et al., 2009) and use the top-1 accuracy on validation set as the evaluation metric. All images are resized to 224. We use the DeiT-base without the distillation token as the default ViT architecture (Touvron et al., 2021). We consider three types of quantization precision: 1) binary weights, and full-precision activations (W1A32); 2) binary weights, and 8-bit activations (W1A8); 3) binary weights, and 6-bit activations (W1A6).

Training We strictly follow the training settings in (Touvron et al., 2021) for all the three training stages. In detail,

the network is trained for 300 epochs and is optimized by AdamW (Loshchilov & Hutter, 2019) with weight decay 0.05. The batch size is set to 512, The learning rate is set to 5×10^{-4} initially and is decayed with a cosine annealing schedule. All data augmentations in (Touvron et al., 2021) are also included during the training process.

Hardware The ViT accelerators with different precisions are implemented on the Xilinx ZCU102 FPGA platform with 2520 DSPs and 274k LUTs, while VAQF can be generalized to other types of FPGAs. For all the implementations, the operating frequency is set to 150 MHz to maximize the computation efficiency and avoid timing violation. The hardware implementations are preformed with the HLS tool of Xilinx Vivado 2020.1.

6.2. Results on Software

6.2.1. COMPARISON WITH OTHER LIGHTWEIGHT ViTs

We first compare our quantized DeiT-base with other lightweight ViTs that are trained from scratch on the ImageNet-1K dataset. All the models are trained without additional distillation. We also report the space usage of devices for each model/method, which is calculated as the product of the number of parameters and the precision. All results are shown in Table 2. Firstly, all other lightweight ViTs are still full-precision models, while the weights in our method are all binarized. It can be seen that with binarized weight, it is feasible to consume much less storage space of devices without changing the original network architecture. Secondly, compared with the full-precision DeiT-base, our weight-binarized version only drops 2.3% accuracy (from 81.8% to 79.5 %). When further quantizing the activations to low percision, the accuracy can still maintain 77.6% for 8-bit and 76.5% for 6-bit, which is still much better than other lightweight ViTs. Although quantizing the activations does not reduce the model size on devices, it can reduce the inference time on the hardware. More details of the efficiency evaluation will be discussed in Section 6.3.

Table 2. Comparison of ViT variants on ImageNet validation set.

Method	Accuracy (%)	Space Usage
DeiT-base	81.8	86M \times 32
T2T (Yuan et al., 2021b)	71.7	4.7M \times 32
DeiT (Touvron et al., 2021)	72.2	5.7M \times 32
PiT (Heo et al., 2021)	73.0	4.9M \times 32
Cross-ViT (Chen et al., 2021a)	73.4	6.9M \times 32
MobileViT (Mehta & Rastegari, 2021)	74.8	2.3M \times 32
Ours (DeiT-base-W1A32)	79.5	86M \times 1
Ours (DeiT-base-W1A8)	77.6	86M \times 1
Ours (DeiT-base-W1A6)	76.5	86M \times 1

6.2.2. ABLATION STUDIES

Architecture of ViT Besides DeiT-base, we also evaluate the accuracy of mix-quantization on DeiT-tiny and DeiT-small (Touvron et al., 2021) on ImageNet. In detail, the number of parameters of DeiT-tiny is 5 million, and that of DeiT-small is 22 million, due to the smaller number of embedding dimension and fewer heads. Table 3 presents the comparison between the full-precision model (W32A32) and the model with binary weights and full-precision activations (W1A32). Different from the DeiT-base, after binarizing their weights, the accuracy of both DeiT-tiny and DeiT-small drop heavily. We hypothesize that these lightweight networks are very fragile as the number of parameters is quite limited. As a consequence, when binarizing their weights, the learning capacity is heavily restricted and thus it is challenging to learn the spatial inductive bias for vision from scratch (Dosovitskiy et al., 2020). Therefore, it is difficult to binarize these lightweight ViTs and maintain their accuracy.

Table 3. Accuracy (%) of mix-quantization DeiT-tiny and DeiT-small on ImageNet validation set.

Quantization Precision	DeiT-tiny	DeiT-small
W32A32	72.2	79.9
W1A32	51.5	70.4

Training Schedules In this section, we aim to show the effect of three-stage training steps and progressive binarization strategy. Due to the computing limitation, we randomly sample 100 categories from the full ImageNet datasets (named “ImageNet-100”), and conduct the ablation studies on this subset. Specifically, we take 32-bit pre-training or progressive binary training out of the training procedure to evaluate the effectiveness of each strategy. Table 4 shows the ablation results. All the results are based on DeiT-small architecture. Remarkably, without the full-precision pre-training, there is a huge drop of accuracy. When further removing the progressive binarization, there is an additional 0.9% accuracy drop. These results verify the effectiveness of our proposed stage-wise finetuning strategy and progressive binarization.

Table 4. Ablation studies on ImageNet-100 validation set.

Method	Accuracy (%)
W1A32	84.3
W1A32 (w/o pre-training)	79.3
W1A32 (w/o progressive)	78.4

Table 5. Hardware resource utilization and performance of ViT accelerators with different frame rates and precisions.

Quantization Precision	Resource Utilization				FPS	Throughput (GOPS)	GOPS/DSP	GOPS/kLUT
	DSP	kLUT	BRAM36	kFF				
W32A32	1564 (62%)	120 (44%)	453.5 (50%)	99 (18%)	10.0	345.8	0.221	2.882
W1A8	1564 (62%)	143 (52%)	565.5 (62%)	110 (20%)	24.8	861.2	0.551	6.022
W1A6	673 (27%)	166 (60%)	392.5 (43%)	82 (15%)	31.6	1096	1.628	6.599

Table 6. Performance comparison among FPGA accelerators, CPU and GPU.

Performance \ Implementation	CPU	GPU	(Liu et al., 2021b) for BERT		Ours for DeiT-base		
	i7-9800X	TITAN RTX	ZCU102	ZCU111	W32A32	W1A8	W1A6
FPS	15.3	183.4	22.8	42.0	10.0	24.8	31.6
Power (W)	100	260	9.8	13.2	9.9	8.7	7.8
Energy Efficiency (FPS/W)	0.15	0.71	2.32	3.18	1.01	2.85	4.05

6.3. Results on Hardware

6.3.1. RESOURCE UTILIZATION AND PERFORMANCE OF ViT ACCELERATORS

Table 5 summarizes the resource utilization and performance of the VAQF-generated ViT accelerators with various frame rates and precisions on FPGAs. The quantization precision is represented by $W[q_w]A[q_a]$, where q_w is the bit-length for weights and q_a the bit-length for activations. For quantized models, the precision on hardware is the same as that on software, while for unquantized models, the parameters and activations in W32A32 precision on software are represented with W16A16 precision on hardware to reduce the computation and storage resource utilization without accuracy loss. The utilization of resources on FPGA is shown with the percentage of the used and total available number. The numbers of LUTs and FFs are expressed as thousands, and the number of BRAMs is listed treating the capacity of each BRAM as 36k bits. The performance of ViT implementations are obtained from the inference process of DeiT-base in terms of the frame rate in FPS, the throughput in giga operations per second (GOPS), and computation efficiency including GOPS per DSP and GOPS per thousands of LUTs.

The inference speed of the W1A8 design is 24.8 FPS, and that for W1A6 is 31.6 FPS. Compared with the baseline implementation with W32A32, these two designs respectively achieve $2.48\times$ and $3.16\times$ acceleration. In these low-precision accelerators, the parallelism in unquantized computations is degraded because of the reduction of DSP utilization, while that in quantized computations is enhanced since more LUTs are utilized. This assists the accelerators to attain higher overall throughput and better fit into the available computation resources, avoiding placement and routing issues. Higher throughput and lower DSP utilization results in $2.49\times$ higher GOPS/DSP of the W1A8 design than the W32A32 one, and this ratio for W1A6 can reach

$7.37\times$. With slightly more LUT utilization for the quantized operations and extra logic to select between unquantized or quantized operations, the GOPS/kLUT increases by $2.09\times$ and $2.29\times$ for W1A8 and W1A6 designs, respectively.

These experimental results demonstrate that the accelerators generated by VAQF are able to achieve real-time inferences, i.e., a frame rate requirement of 24 FPS is satisfied with 8-bit quantization for activations, and a target of 30 FPS is met with 6-bit activation quantization. VAQF can be further generalized to other frame rate targets and other types of transformers.

6.3.2. COMPARISON WITH OTHER IMPLEMENTATIONS

Our accelerators are further compared with previous work, CPU and GPU with regard to FPS, power, and energy efficiency. Since no study using quantization has been carried out for ViT acceleration on FPGAs, the accelerators for BERT in (Liu et al., 2021b) with 8×4 -bit and 8×8 -bit quantization are used for comparison, and other implementation results are all obtained for DeiT-base. As shown in Table 6, our W1A8 and W1A6 accelerators both outperform the BERT design on ZCU102 in terms of FPS, power and energy efficiency, and the W1A6 design has the highest FPS/W among all implementations. Compared with the inferences on Intel(R) Core(TM) i7-9800X CPU and NVIDIA TITAN RTX GPU, our W1A6 design has $27.0\times$ and $5.7\times$ improvement in FPS/W.

7. Conclusion

This work proposes a framework called VAQF for automatic construction of inference accelerators for ViTs with binary weights and low-precision activations under the desired frame rate. VAQF first performs compilation to decide the required activation precision with the accelerator settings related to the computation parallelism by analyzing the resource utilization and inference performance. And then for

the accelerator implementation, a compute engine general for FC layers and multi-head attention layers is designed, and the quantized computations are replaced with additions and subtractions that are implemented with LUTs. Optimization techniques like data packing and loop pipelining are utilized with different factors for unquantized and quantized computations to enhance the computation parallelism and memory utilization efficiency. The experimental results for the DeiT-base model show that the accelerator with 8-bit activation quantization achieves an inference speed of 24.8 FPS, and that with 6-bit activation quantization attains 31.6 FPS, which can meet various real-time requirements.

References

- Bai, H., Zhang, W., Hou, L., Shang, L., Jin, J., Jiang, X., Liu, Q., Lyu, M., and King, I. Binarybert: Pushing the limit of bert quantization. *arXiv preprint arXiv:2012.15701*, 2020.
- Bao, H., Dong, L., and Wei, F. Beit: Bert pre-training of image transformers. *arXiv preprint arXiv:2106.08254*, 2021.
- Brown, T. B., Mann, B., Ryder, N., Subbiah, M., Kaplan, J., Dhariwal, P., Neelakantan, A., Shyam, P., Sastry, G., Askell, A., et al. Language models are few-shot learners. *arXiv preprint arXiv:2005.14165*, 2020.
- Carion, N., Massa, F., Synnaeve, G., Usunier, N., Kirillov, A., and Zagoruyko, S. End-to-end object detection with transformers. In *European Conference on Computer Vision*, pp. 213–229. Springer, 2020.
- Chen, C.-F., Fan, Q., and Panda, R. Crossvit: Cross-attention multi-scale vision transformer for image classification. *arXiv preprint arXiv:2103.14899*, 2021a.
- Chen, M., Peng, H., Fu, J., and Ling, H. Autoformer: Searching transformers for visual recognition. *arXiv preprint arXiv:2107.00651*, 2021b.
- Chen, T., Frankle, J., Chang, S., Liu, S., Zhang, Y., Wang, Z., and Carbin, M. The lottery ticket hypothesis for pre-trained bert networks. *arXiv preprint arXiv:2007.12223*, 2020.
- Chen, T., Cheng, Y., Gan, Z., Yuan, L., Zhang, L., and Wang, Z. Chasing sparsity in vision transformers: An end-to-end exploration. *arXiv preprint arXiv:2106.04533*, 2021c.
- Chen, X., Hsieh, C.-J., and Gong, B. When vision transformers outperform resnets without pretraining or strong data augmentations. *arXiv preprint arXiv:2106.01548*, 2021d.
- Deng, J., Dong, W., Socher, R., Li, L.-J., Li, K., and Fei-Fei, L. Imagenet: A large-scale hierarchical image database. In *2009 IEEE conference on computer vision and pattern recognition*, pp. 248–255. Ieee, 2009.
- Dosovitskiy, A., Beyer, L., Kolesnikov, A., Weissenborn, D., Zhai, X., Unterthiner, T., Dehghani, M., Minderer, M., Heigold, G., Gelly, S., et al. An image is worth 16x16 words: Transformers for image recognition at scale. *arXiv preprint arXiv:2010.11929*, 2020.
- El-Nouby, A., Touvron, H., Caron, M., Bojanowski, P., Douze, M., Joulin, A., Laptev, I., Neverova, N., Synnaeve, G., Verbeek, J., et al. Xcit: Cross-covariance image transformers. *arXiv preprint arXiv:2106.09681*, 2021.
- Graham, B., El-Nouby, A., Touvron, H., Stock, P., Joulin, A., Jégou, H., and Douze, M. Levit: a vision transformer in convnet’s clothing for faster inference. *arXiv preprint arXiv:2104.01136*, 2021.
- Han, K., Xiao, A., Wu, E., Guo, J., Xu, C., and Wang, Y. Transformer in transformer. *arXiv preprint arXiv:2103.00112*, 2021.
- Heo, B., Yun, S., Han, D., Chun, S., Choe, J., and Oh, S. J. Rethinking spatial dimensions of vision transformers. *arXiv preprint arXiv:2103.16302*, 2021.
- Jiang, Z., Hou, Q., Yuan, L., Zhou, D., Shi, Y., Jin, X., Wang, A., and Feng, J. All tokens matter: Token labeling for training better vision transformers. *arXiv preprint arXiv:2104.10858*, 2021.
- Jiao, X., Yin, Y., Shang, L., Jiang, X., Chen, X., Li, L., Wang, F., and Liu, Q. Tinybert: Distilling bert for natural language understanding. *arXiv preprint arXiv:1909.10351*, 2019.
- Li, B., Pandey, S., Fang, H., Lyv, Y., Li, J., Chen, J., Xie, M., Wan, L., Liu, H., and Ding, C. Ftrans: energy-efficient acceleration of transformers using fpga. In *Proceedings of the ACM/IEEE International Symposium on Low Power Electronics and Design*, pp. 175–180, 2020.
- Li, K., Wang, S., Zhang, X., Xu, Y., Xu, W., and Tu, Z. Pose recognition with cascade transformers. *arXiv preprint arXiv:2104.06976*, 2021.
- Lin, K., Wang, L., and Liu, Z. End-to-end human pose and mesh reconstruction with transformers. *arXiv preprint arXiv:2012.09760*, 2020.
- Liu, Y., Sangineto, E., Bi, W., Sebe, N., Lepri, B., and De Nadai, M. Efficient training of visual transformers with small-size datasets. *arXiv preprint arXiv:2106.03746*, 2021a.

- Liu, Z., Shen, Z., Savvides, M., and Cheng, K.-T. Reactnet: Towards precise binary neural network with generalized activation functions. In *European Conference on Computer Vision*, pp. 143–159. Springer, 2020.
- Liu, Z., Li, G., and Cheng, J. Hardware acceleration of fully quantized bert for efficient natural language processing. *arXiv preprint arXiv:2103.02800*, 2021b.
- Liu, Z., Lin, Y., Cao, Y., Hu, H., Wei, Y., Zhang, Z., Lin, S., and Guo, B. Swin transformer: Hierarchical vision transformer using shifted windows. *arXiv preprint arXiv:2103.14030*, 2021c.
- Liu, Z., Wang, Y., Han, K., Ma, S., and Gao, W. Post-training quantization for vision transformer. *arXiv preprint arXiv:2106.14156*, 2021d.
- Loshchilov, I. and Hutter, F. Decoupled weight decay regularization. In *International Conference on Learning Representations*, 2019. URL <https://openreview.net/forum?id=Bkg6RiCqY7>.
- Mehta, S. and Rastegari, M. Mobilevit: Light-weight, general-purpose, and mobile-friendly vision transformer. *arXiv preprint arXiv:2110.02178*, 2021.
- Michel, P., Levy, O., and Neubig, G. Are sixteen heads really better than one? *arXiv preprint arXiv:1905.10650*, 2019.
- Peng, H., Huang, S., Geng, T., Li, A., Jiang, W., Liu, H., Wang, S., and Ding, C. Accelerating transformer-based deep learning models on fpgas using column balanced block pruning. In *2021 22nd International Symposium on Quality Electronic Design (ISQED)*, pp. 142–148. IEEE, 2021.
- Prato, G., Charlaix, E., and Rezagholizadeh, M. Fully quantized transformer for improved translation. 2019.
- Qi, P., Song, Y., Peng, H., Huang, S., Zhuge, Q., and Sha, E. H.-M. Accommodating transformer onto fpga: Coupling the balanced model compression and fpga-implementation optimization. In *Proceedings of the 2021 on Great Lakes Symposium on VLSI*, pp. 163–168, 2021.
- Radford, A., Wu, J., Child, R., Luan, D., Amodei, D., Sutskever, I., et al. Language models are unsupervised multitask learners.
- Raghu, M., Unterthiner, T., Kornblith, S., Zhang, C., and Dosovitskiy, A. Do vision transformers see like convolutional neural networks? *arXiv preprint arXiv:2108.08810*, 2021.
- Rastegari, M., Ordonez, V., Redmon, J., and Farhadi, A. Xnor-net: Imagenet classification using binary convolutional neural networks. In *European conference on computer vision*, pp. 525–542. Springer, 2016.
- Sanh, V., Debut, L., Chaumond, J., and Wolf, T. Distilbert, a distilled version of bert: smaller, faster, cheaper and lighter. *arXiv preprint arXiv:1910.01108*, 2019.
- Shen, S., Dong, Z., Ye, J., Ma, L., Yao, Z., Gholami, A., Mahoney, M. W., and Keutzer, K. Q-bert: Hessian based ultra low precision quantization of bert. In *Proceedings of the AAAI Conference on Artificial Intelligence*, volume 34, pp. 8815–8821, 2020.
- Steiner, A., Kolesnikov, A., Zhai, X., Wightman, R., Uszkoreit, J., and Beyer, L. How to train your vit? data, augmentation, and regularization in vision transformers, 2021.
- Sun, S., Cheng, Y., Gan, Z., and Liu, J. Patient knowledge distillation for bert model compression. *arXiv preprint arXiv:1908.09355*, 2019.
- Touvron, H., Cord, M., Douze, M., Massa, F., Sablayrolles, A., and J’egou, H. Training data-efficient image transformers & distillation through attention. In *ICML*, 2021.
- Vaswani, A., Shazeer, N., Parmar, N., Uszkoreit, J., Jones, L., Gomez, A. N., Kaiser, Ł., and Polosukhin, I. Attention is all you need. In *Advances in neural information processing systems*, pp. 5998–6008, 2017.
- Wang, P., Wang, X., Wang, F., Lin, M., Chang, S., Xie, W., Li, H., and Jin, R. Kvt: k-nn attention for boosting vision transformers, 2021a.
- Wang, W., Xie, E., Li, X., Fan, D.-P., Song, K., Liang, D., Lu, T., Luo, P., and Shao, L. Pyramid vision transformer: A versatile backbone for dense prediction without convolutions. *arXiv preprint arXiv:2102.12122*, 2021b.
- Wang, Y., Xu, Z., Wang, X., Shen, C., Cheng, B., Shen, H., and Xia, H. End-to-end video instance segmentation with transformers. *arXiv preprint arXiv:2011.14503*, 2020.
- Wu, K., Peng, H., Chen, M., Fu, J., and Chao, H. Rethinking and improving relative position encoding for vision transformer, 2021.
- Yuan, K., Guo, S., Liu, Z., Zhou, A., Yu, F., and Wu, W. Incorporating convolution designs into visual transformers, 2021a.
- Yuan, L., Chen, Y., Wang, T., Yu, W., Shi, Y., Jiang, Z., Tay, F. E., Feng, J., and Yan, S. Tokens-to-token vit: Training vision transformers from scratch on imagenet. *arXiv preprint arXiv:2101.11986*, 2021b.
- Yue, X., Sun, S., Kuang, Z., Wei, M., Torr, P., Zhang, W., and Lin, D. Vision transformer with progressive sampling. *arXiv preprint arXiv:2108.01684*, 2021.

- Zafri, O., Boudoukh, G., Izsak, P., and Wasserblat, M. Q8bert: Quantized 8bit bert. *arXiv preprint arXiv:1910.06188*, 2019.
- Zhang, W., Hou, L., Yin, Y., Shang, L., Chen, X., Jiang, X., and Liu, Q. Ternarybert: Distillation-aware ultra-low bit bert. *arXiv preprint arXiv:2009.12812*, 2020.
- Zheng, S., Lu, J., Zhao, H., Zhu, X., Luo, Z., Wang, Y., Fu, Y., Feng, J., Xiang, T., Torr, P. H., et al. Rethinking semantic segmentation from a sequence-to-sequence perspective with transformers. *arXiv preprint arXiv:2012.15840*, 2020.
- Zhu, X., Su, W., Lu, L., Li, B., Wang, X., and Dai, J. Deformable detr: Deformable transformers for end-to-end object detection. *arXiv preprint arXiv:2010.04159*, 2020.